Mon. Not. R. Astron. Soc. **000**, 000–000 (0000) Printed 11 September 2012 (MN LATEX style file v2.2)

The Radio Signatures of the First Supernovae

Avery Meiksin[1], Daniel J. Whalen[2]
SUPA, [1] Institute for Astronomy, University of Edinburgh, Blackford Hill, Edinburgh EH9 3HJ, UK*
[2] McWilliams Fellow, Department of Physics, Carnegie-Mellon University, Pittsburgh, PA 15213, USA

11 September 2012

ABSTRACT

Primordial stars are key to primeval structure formation as the first stellar components of primeval galaxies, the sources of cosmic chemical enrichment and likely cosmic reionization, and they possibly gave rise to the supermassive black holes residing at the centres of galaxies today. While the direct detection of individual Pop III stars will likely remain beyond reach for decades to come, we show their supernova remnants may soon be detectable in the radio. We calculate radio synchrotron signatures between $0.5-35$ GHz from hydrodynamical computations of the supernova remnants of Pop III stars in minihaloes. We find that hypernovae yield the brightest systems, with observed radio fluxes as high as $1-10\,\mu$Jy. Less energetic Type II supernovae yield remnants about a factor of 30 dimmer and pair-instability supernova remnants are dimmer by a factor of more than 10,000. Hypernovae radio remnants should be detectable by existing radio facilities like eVLA and eMERLIN while Type II supernova remnants will require the Square Kilometre Array. The number counts of hypernova remnants at $z > 20$ with fluxes above $1\,\mu$Jy are expected to be one per fifty square degree field, increasing to a few per square degree if they form down to $z = 10$. The detection of a $z > 20$ Type II supernova remnant brighter than 1 nJy would require a 200–300 square degree field, although only a 1–2 square degree field for those forming down to $z = 10$. Hypernova and Type II supernova remnants are easily distinguishable from one another by their light curves, which will enable future surveys to use them to constrain the initial mass function of Pop III stars.

Key words: radiation mechanisms: non-thermal – supernovae: general – galaxies: formation – cosmology: theory – radio continuum: galaxies

1 INTRODUCTION

The cosmic Dark Ages ended with the formation of the first stars in $10^5 - 10^6\,\mathrm{M}_\odot$ cosmological haloes at $z \sim 20-30$. Primordial (or Pop III) stars are the key to understanding primeval galaxies, the onset of early cosmological reionization and chemical enrichment, and the origins of the supermassive black holes found in most massive galaxies today. Unfortunately, in spite of their extreme luminosities (Schaerer 2002) and the arrival of next-generation near infrared (NIR) observatories such as the *James Webb Space Telescope* (*JWST*) and the Thirty-Meter Telescope (TMT), individual Pop III stars will remain beyond the reach of direct detection for decades to come. For now, there are no observational constraints on either their masses or their rates of formation.

On the simulation frontier, there has been a gradual shift in paradigm over the past decade from single $30-300\,\mathrm{M}_\odot$ stars forming in isolation in haloes (Bromm et al. 2002; Nakamura & Umemura 2001; Abel et al. 2002; O'Shea & Norman 2007, 2008; Wise & Abel 2007) to binaries (Turk et al. 2009) and more recently to the possibility of $20-40\,\mathrm{M}_\odot$ stars forming in small multiples of up to a dozen (Stacy et al. 2010; Clark et al. 2011; Greif et al. 2011; Hosokawa et al. 2011; Stacy et al. 2011; Greif et al. 2012). However, these simulations do not estimate Pop III stellar masses by modeling the formation and evolution of the stars. Instead, they usually derive them by comparing infall rates at the center of the halo at very early stages of collapse to Kelvin-Helmholz contraction times to place upper limits on the final mass of the star. No simulation currently bridges the gap between the initial formation and fragmentation of a protostellar disk and its photoevaporation up to a Myr later, so there are no firm numerical constraints on the Pop III IMF either (see Whalen 2012, for a recent review of primordial star formation).

Pop III stars profoundly transformed the haloes that gave birth to them, driving out most of their baryons in supersonic ionized flows (Whalen et al. 2004; Kitayama et al.

* Scottish Universities Physics Alliance

2004; Alvarez et al. 2006; Abel et al. 2007) and later exploding as supernovae (SNe) (Bromm et al. 2003; Kitayama & Yoshida 2005; Greif et al. 2007; Whalen et al. 2008). Ionization fronts from these stars also engulfed nearby haloes, either promoting or suppressing star formation in them and regulating the rise of the first stellar populations (e.g. Shapiro et al. 2004; Iliev et al. 2005; Susa & Umemura 2006; Whalen et al. 2008; Hasegawa et al. 2009; Susa et al. 2009; Whalen et al. 2010). As each halo hosted consecutive cycles of stellar birth, H II region formation and SN explosions (Yoshida et al. 2007), gravity and accretion flows congregated them into the first primitive galaxies with halo merger time-scales of ~ 20 Myr at $z \sim 20$ (e.g. Johnson et al. 2008; Greif et al. 2008, 2010; Wise et al. 2012). At the same time, the first SNe enriched the IGM with metals and dust, triggering a transition from Pop III to Pop II star formation (e.g. Mackey et al. 2003; Smith & Sigurdsson 2007; Smith et al. 2009; Nagakura et al. 2009; Chiaki et al. 2012). How these two processes determined the masses and formation rates of stars in primeval galaxies at $z \sim 10 - 15$, and therefore their spectra and luminosities, is unknown.

Stellar evolution models show that the final fates of the first stars rested upon their masses at birth (Heger & Woosley 2002): $15 - 40\,\mathrm{M}_\odot$ Pop III stars died in core-collapse SNe (Joggerst et al. 2010) and $40 - 140\,\mathrm{M}_\odot$ stars collapsed to black holes, perhaps with violent pulsational mass loss prior to death (Woosley et al. 2007). Pop III stars from 140 to 260 $\mathrm{M}_\odot$ died as pair instability (PI) SNe, extremely energetic thermonuclear explosions with energies of up to 100 those of Type Ia and Type II SNe (Joggerst & Whalen 2011; Chatzopoulos & Wheeler 2012 extend this lower limit down to $65\,\mathrm{M}_\odot$ for rotating stars). Some $40 - 60\,\mathrm{M}_\odot$ Pop III stars may have died as hypernovae, with energies intermediate to those of core-collapse and PI SNe (Iwamoto et al. 2005). Attempts have been made to indirectly constrain the masses of the first stars by reconciling the cumulative nucleosynthetic yield of their supernovae to the chemical abundances found in ancient, dim metal-poor stars in the Galactic halo (Beers & Christlieb 2005; Frebel et al. 2005), some of which may be contaminated with the ashes of the first generation. For example, Joggerst et al. (2010) recently discovered that the average yields of $15 - 40\,\mathrm{M}_\odot$ Pop III SNe agree well with the fossil abundances measured in ~ 130 stars with metallicities $Z < 10^{-4} Z_\odot$ (Cayrel et al. 2004; Lai et al. 2008), suggesting that low-mass primordial stars may have synthesized most metals at high redshift. However, stellar archaeology is still in its infancy because of small sample sizes, systematics in the measurements of some elements, and because the imprint of metals from first-generation stars on the second is not well understood.

The direct detection of Pop III SNe may be the best prospect for probing the earliest generation of stars in the near term. Primordial supernovae may be 100,000 times brighter than their progenitors, or, at slightly lower redshifts, the primitive galaxies in which they reside. Their transience easily distinguishes them from early galaxies, with which they otherwise overlap in colour–colour space. Previous studies have investigated detection limits for PI SNe at $z \sim 6$ (Scannapieco et al. 2005; Tanaka et al. 2012), for $6 < z < 15$ (Pan et al. 2011; Moriya et al. 2012, Whalen, Joggerst et al. in preparation; Whalen, Even et al. in preparation), and in very approximate terms for $z \sim 30$ (Hummel et al. 2012). Whalen, Fryer et al. (in preparation) and Whalen, Frey et al. (in preparation) show that *JWST* will detect PI SNe beyond $z \sim 30$ and that the *Wide Field Infrared Survey Telescope* (*WFIRST*) and the *Wide-field Imaging Surveyor for High-Redshift* (*WISH*) will detect them out to $z \sim 15 - 20$ in all-sky NIR surveys. Unfortunately, it may be a decade before such observations are possible, given that *JWST* and *WFIRST* will not be in operation before 2018 and 2021, respectively.

In the meantime, it may be possible to discover the first generation of supernovae in cosmic backgrounds. Pair instability SNe deposit up to half of their energy into the CMB via inverse Compton scattering at $z \sim 20$ (Kitayama & Yoshida 2005; Whalen et al. 2008). Oh et al. (2003) have found that Pop III PI SNe may impose excess power on the CMB on small scales via the Sunyayev-Zeldovich effect. Primordial SNe may also be manifest as fluctuations in the NIR background because they are so much more luminous than their host protogalaxies at high redshift. In this paper, we show Pop III supernovae may also be revealed through the detection of the radio emission from their remnants by both current and future radio observatories such as the eVLA[1], eMERLIN[2], ASKAP[3] and the Square Kilometre Array[4] (SKA).

Previous studies of the observability of collapsing structures at $z > 10$ in the radio have centered on detecting the 21cm signal of minihaloes during the cosmic dark ages (e.g. Furlanetto & Loeb 2002; Iliev et al. 2002; Shapiro et al. 2006; Meiksin 2011), not cosmic explosions at first light. There are several advantages to searching for the first supernovae through their radio synchrotron emission. Firstly, if only certain types of explosions contribute a radio signal, this may be used to place limits on the masses of their progenitors. Secondly, supernova (and hence star formation) rates may possibly be determined from the strength of the radio signals and the number counts of the sources. Finally, depending on the properties of this signal, it may be possible to pinpoint the redshift of the explosions. In this paper we calculate the radio signal produced by the remnants of core-collapse SNe, hypernovae and PI SNe to assess the detectability of the remnants by current and future observatories. We also determine if this signal may constrain the masses and formation rates of Pop III stars in high redshift protogalaxies. In § 2 we review how Pop III SN explosions generate synchrotron emission that could be directly detected by current and planned radio telescopes. In § 3 we describe the expected radio light curves and number counts of the Pop III SN radio remnants. We summarise our conclusions in § 4. Formulae are provided for synchrotron emission and self-absorption in terms of the energy densities of the relativistic electrons and the magnetic field in an appendix.

For numerical cosmological estimates, we adopt $\Omega_\mathrm{m} = 0.27$, $\Omega_\mathrm{v} = 0.73$, $H_0 = 100\,\mathrm{km\,s^{-1}\,Mpc^{-1}}$, $\sigma_{8\mathrm{h}^{-1}} = 0.81$ and $n = 0.96$ for the total mass and vacuum energy density parameters, the Hubble constant, the linear den-

[1] www.aoc.nrao.edu/evla/
[2] www.jb.man.ac.uk/research/rflabs/eMERLIN.html
[3] www.atnf.csiro.au/projects/askap
[4] www.skatelescope.org

sity fluctuation amplitude on a scale of $8\,h^{-1}$Mpc and the spectral index, respectively, consistent with the best-fitting cosmological parameters for a flat universe as constrained by the 5-yr *Wilkinson Microwave Anisotropy Probe* (*WMAP*) measurements of the Cosmic Microwave Background (Komatsu et al. 2009).

2 THE SYNCHROTRON SIGNATURE OF SUPERNOVAE IN MINI-HALOES

We begin by estimating the expected synchrotron flux from a supernova remnant. For relativistic electrons in a magnetic field of energy density u_B, the bolometric emissivity of synchrotron radiation is

$$\epsilon_{\rm bol} \sim u_B \tau_{\rm se}^{-1}, \quad (1)$$

where $\tau_{\rm se}$ is the characteristic energy scattering time-scale for electrons of energy density u_e, defined by

$$\tau_{\rm se} = \frac{m_e c^2}{c\sigma_T u_e}. \quad (2)$$

Here σ_T is the Thomson cross section for electron scattering and m_e is the mass of an electron.

Allowing for a fraction f_e of the thermal energy to go into relativistic electrons, so that $u_e = f_e u_{\rm th}$ for a thermal energy density $u_{\rm th}$, and further assuming equipartition $u_B \simeq u_e$(Chevalier 1982), the bolometric synchrotron power emitted by a single halo is

$$P_{\rm bol}^{\rm sync} \simeq 4\pi \frac{c\sigma_T}{m_e c^2} \int dr r^2 f_e(r)^2 u_{\rm th}^2 F(p_e; \gamma_l, \gamma_u), \quad (3)$$

where the function $F(p_e; \gamma_l, \gamma_u)$, described in the Appendix, allows for a power-law energy distribution of index p_e for the relativistic electrons, and γ_l and γ_u are the lower and upper ranges of the relativistic γ factors for the electrons. We generally assume conservatively $\gamma_l = 1$, as non-relativistic electrons will not contribute much synchrotron emission.

We illustrate the expected flux using the computation for a $40\,{\rm M}_\odot$ hypernova in a $1.2 \times 10^7\,{\rm M}_\odot$ halo at $z = 17.3$ (Whalen et al. 2008). The synchrotron power may be estimated from the post-shock thermal energy density of the supernova remnant, which exceeds a few erg cm^{-3} over a region around a tenth of a parsec across during the first $\sim$ 10 yrs. For $f_e = 0.01$ (e.g. Chevalier 1982), this corresponds to a bolometric synchrotron power output of $P_{\rm bol}^{\rm sync} \simeq 5 \times 10^{42}\,{\rm erg\,s^{-1}}$ for $\gamma_u = 300$ and $p = 2$. The spectrum will extend to a lower characteristic cutoff wavelength, assuming an isotropic magnetic field, of $\lambda_c = (2\pi^{1/2}/3)(m_e c^2/e)\gamma_u^{-2} u_B^{-1/2} \simeq 2014 \gamma_u^{-2} u_B^{-1/2}\,{\rm cm} \approx 0.2\,{\rm cm}$, or upper cutoff frequency $\nu_c \simeq 130$ GHz, corresponding to a characteristic specific power at ν_c of $2 \times 10^{31}\,{\rm erg\,s^{-1}\,Hz^{-1}}$. For a source at $z = 17.3$, this corresponds to an observed radio flux of $\sim 10\,\mu$Jy. The flux will vary with frequency as $\nu^{-(p_e-1)/2} = \nu^{-1/2}$.

The radio spectrum computed 4.7 yrs after the explosion is shown in Fig. 1. The free-free radiation is shown as well, but is generally much smaller than the synchrotron. The energy density in relativistic electrons is sufficiently high that synchrotron self-absorption (SSA) is significant at the lower frequencies. Allowing for SSA severely attenuates the spectrum at $\nu \lesssim 20$ GHz, as shown in Fig. 1.

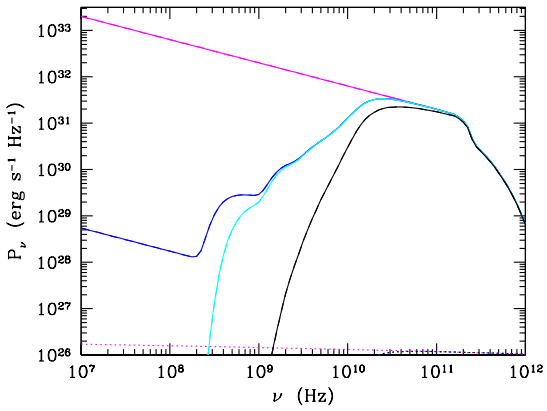

Figure 1. Radio power from a $40\,{\rm M}_\odot$ hypernova in a $1.2{\times}10^7\,{\rm M}_\odot$ minihalo at $z = 17.3$ (for $p_e = 2$, $\gamma_u = 300$ and $f_e = 0.01$). Shown are total (synchrotron and free-free) (solid lines) and free-free (short-dashed lines) powers. The upper curve (magenta) corresponds to a model with no attenuation. The middle curves allow for synchrotron self-absorption (blue) and free-free absorption as well (cyan). The lowest curve (black) further adds hypothesized plasma synchrotron attenuation effects.

Adding free-free absorption degrades the spectrum further at low frequencies. Free-free absorption was neglected from the fluid zone at the shock front, where the gas is becoming ionized but has not yet reached the post-shock temperature. Since the shock front is unresolved, the substantial free-free absorption from it is likely greatly over-estimated. For a shock front width on the order of the Coulomb mean free path, the free-free absorption from the shock front becomes negligible. It will therefore generally not be included here. It is remarked, however, that if cool circumstellar gas mixes in with the post-shock ionized gas, free-free absorption could be non-negligible. Such an effect is beyond the capacity of a spherically symmetric code to reproduce, and would be difficult to resolve in any case.

The Razin-Tsytovich plasma effect on the synchrotron radiation mechanism may further degrade the escaping synchrotron radiation (e.g. Scheuer & Williams 1968; Rybicki & Lightman 1986). We approximate the effect by cutting off the production of synchrotron radiation by the factor $\exp(-\nu_{\rm RT}/\nu)$, where

$$\nu_{\rm RT} = \gamma_u \nu_p \left(1 + \gamma_u \frac{\nu_p}{\nu_c}\right), \quad (4)$$

and ν_p is the electron plasma frequency. This strongly cuts off most of the radiation below $\sim 0.1\nu_c$, as shown in Fig. 1. As the occurrence of the hypothesized effect is unclear, we conservatively neglect it further here, but note that the detection of such greatly diminished low-frequency emission would support its reality.

Radio observations of supernova remnants show a range in values of p_e, typically $1.5 < p_e < 3$, and do not strongly

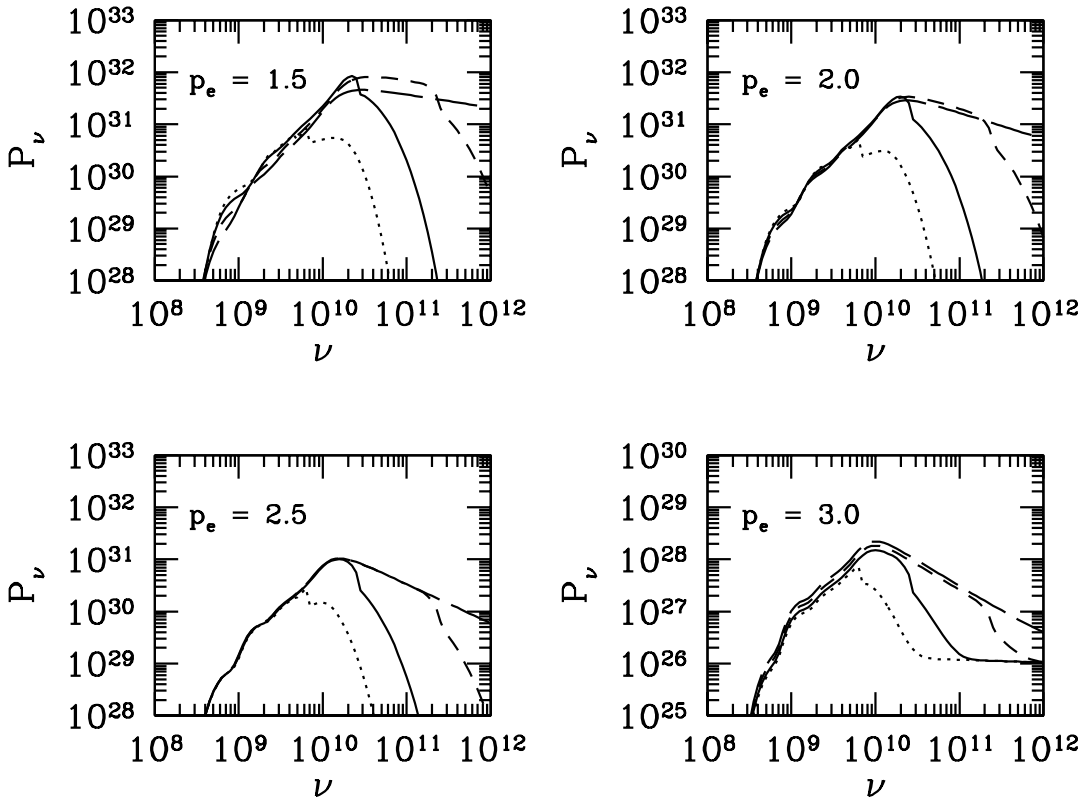

Figure 2. Radio power P_ν (erg s^{-1} Hz^{-1}) as function of emission frequency ν (Hz) from a 40 $M_\odot$ hypernova in a 1.2×10^7 $M_\odot$ minihalo at $z = 17.3$ (for $f_e = 0.01$). The relativistic electron energy power-law index varies over $1.5 < p_e < 3.0$ across the panels. (Note the change in scale for the $p_e = 3.0$ panel.) The power is shown for $\gamma_u = 50$ (dotted lines), 100 (solid lines), 300 (short-dashed lines) and 1000 (long-dashed lines).

constrain γ_u and f_e, although values of $\gamma_u > 100$ and $f_e \sim 0.001 - 0.2$ are indicated (Weiler et al. 1986; Chevalier 1998; Soderberg et al. 2006). The parameters p_e and γ_u are allowed to vary in Fig. 2 for $f_e = 0.01$. The power at $\nu = \nu_c$ is proportional to $f_e^{3/2}$. For a given γ_u, the peak power decreases with increasing p_e. The peak power for a given p_e varies little with γ_u for $\gamma_u > 100$, while increasing γ_u further increases the synchrotron cut-off frequency and so extends the power-law spectrum to higher frequencies. For $p_e \simeq 3$, a substantially larger value of either f_e or the minimum γ factor for the relativistic electrons is required to reproduce the same power as for $f_e < 2.5$.

It is noted that for $f_e = 0.01$, the total synchrotron energy radiated will match the energy in relativistic electrons after a few years. Either γ_u must then decrease with time or f_e must be lower or decrease with time (most likely associated with a steepening of the power-law energy distribution of the relativistic electrons), unless electrons are continuously accelerated to relativistic velocities by the shocks, as is believed to occur in supernova remnants in the Galaxy.

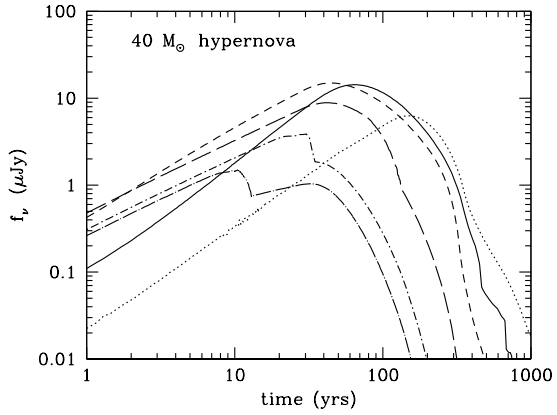

Figure 3. Radio light curves for a $40\,M_\odot$ hypernova in a $1.2 \times 10^7\,M_\odot$ minihalo at $z = 17.3$ (for $p_e = 2$, $\gamma_u = 300$ and $f_e = 0.01$). The observed fluxes are shown for bands: 0.5 (dotted), 1.4 (solid), 3 (short-dashed), 10 (long-dashed), 25 (dot short-dashed) and 35 (dot long-dashed) GHz.

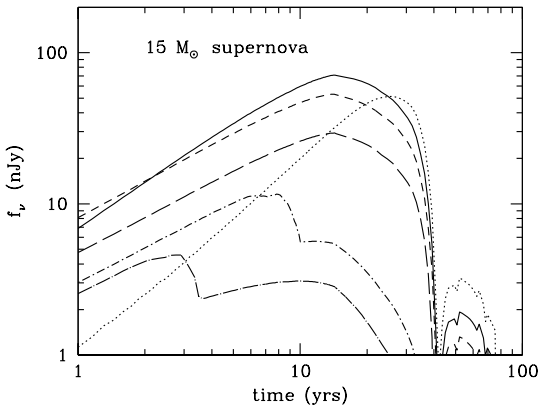

Figure 4. Radio light curves for a $15\,M_\odot$ Type II supernova in a $1.2 \times 10^7\,M_\odot$ minihalo at $z = 17.3$ (for $p_e = 2$, $\gamma_u = 300$ and $f_e = 0.01$). The observed fluxes are shown for bands: 0.5 (dotted), 1.4 (solid), 3 (short-dashed), 10 (long-dashed), 25 (dot short-dashed) and 35 (dot long-dashed) GHz.

3 OBSERVATIONAL PREDICTIONS

Deep radio surveys are currently able to reach the few μJy level. The Very Large Array has achieved an *rms* noise level of $1.5\,\mu$Jy at 8.4 GHz (Fomalont et al. 2002) and $2.7\,\mu$Jy at 1.4 GHz (Owen & Morrison 2008). Similar levels have been reached using eMERLIN (Muxlow et al. 2005). The Square Kilometre Array is projected to be a factor 100–1000 more sensitive.

In Figs 3 and 4, we show the light curves for a $40\,M_\odot$ hypernova and $15\,M_\odot$ Type II supernova, respectively, in a $1.2 \times 10^7\,M_\odot$ minihalo at $z = 17.3$ in selected bands planned for the SKA. The bands lie within the eVLA frequency range. The eMERLIN L-band includes 1.4 GHz, while the C-band flux light curve would lie between those for the 3 and 10 GHz bands. Time-dilation produces a gradual rise extended over a 100 yr time-scale with an even slower decline. For the $40\,M_\odot$ hypernova, a flux exceeding $1\,\mu$Jy is expected to persist over a span of 300 yrs, with a peak flux of $\sim 10\,\mu$Jy. Most notable is the relatively late rise of the flux in the 500 MHz band; it eventually overtakes the higher frequency fluxes for a period of 200 yrs while above $1\,\mu$Jy. A similar trend is found for the $15\,M_\odot$ supernova, although over the much shorter time-scale of decades and with flux values lower by 1.5 dex. We also computed the emission following a $260\,M_\odot$ pair instability supernova, but found it so efficiently sweeps through the minihalo that the resulting observed radio flux is at most ~ 0.1 nJy. Similarly, we found the observed radio fluxes from the remnants produced in a $2 \times 10^6\,M_\odot$ halo by all three supernova progenitor masses fell well below 1 nJy.

Allowing for the Razin-Tsytovich effect much reduces the flux in the 500 MHz band, as shown in Fig. 5. While it continues to rise with time, it lies about 1 dex below the flux

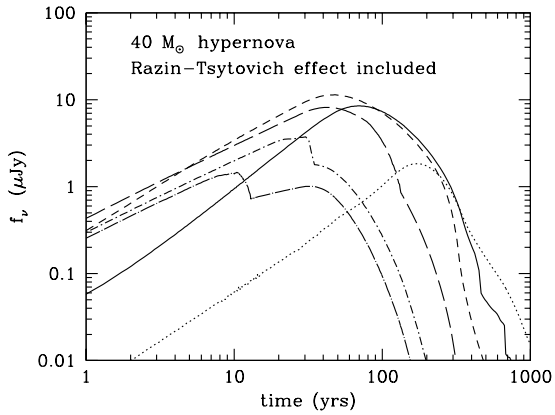

Figure 5. Radio light curves for a $40\,M_\odot$ hypernova in a $1.2 \times 10^7\,M_\odot$ minihalo at $z = 17.3$ (for $p_e = 2$, $\gamma_u = 300$ and $f_e = 0.01$). The Razin-Tsytovich effect is included. The observed fluxes are shown for bands: 0.5 (dotted), 1.4 (solid), 3 (short-dashed), 10 (long-dashed), 25 (dot short-dashed) and 35 (dot long-dashed) GHz.

at 1.4 GHz for 350 yrs. When it does overtake the 1.4 GHz flux, its value lies well below 1 μJy. Comparison with Fig. 3 suggests the measured flux in the 500 MHz band may be used to detect the presence of the Razin-Tsytovich effect.

The number of sources visible per year is substantial. We estimate this from the halo collapse rate using the halo fitting function of Reed et al. (2007), adapted to the 5 yr *WMAP* cosmological parameters for a flat universe (Komatsu et al. 2009). The observed formation rate of haloes within a solid angle $\delta\Omega$ with a comoving number density $n_h^{\rm com}(z)$ for halo masses exceeding M_h, integrated over $z_1 < z < z_2$, is then

$$\begin{aligned}\dot{N}_h^{\rm obs}(>M_h) &= \int_{z_1}^{z_2} dz\, \dot{n}_h^{\rm com}(1+z)^3 \frac{dV^{\rm prop}}{dz}\frac{1}{1+z}\\ &= -\int_{z_1}^{z_2} dz\, \frac{dn_h^{\rm com}}{dz} c(a_0 r)^2 \delta\Omega\\ &= \left[n_h^{\rm com} c(a_0 r)^2\right]_{z_2}^{z_1}\delta\Omega\\ &\quad +2\left(\frac{c}{H_0}\right)\int_{z_1}^{z_2} dz\, n_h^{\rm com} c \frac{a_0 r}{[\Omega_{\rm m}(1+z)^3+\Omega_{\rm v}]^{1/2}}\delta\Omega\\ &\simeq n_h^{\rm com}(z_1) c[a_0 r(z_1)]^2\delta\Omega, \end{aligned} \quad (5)$$

where $a_0 r(z) = (c/H_0)\int_0^z dz\,[\Omega_{\rm m}(1+z)^3+\Omega_{\rm v}]^{-1/2}$ is the angular size distance for a flat universe with present day mass and vacuum energy density parameters $\Omega_{\rm m}$ and $\Omega_{\rm v}$, respectively, and Hubble constant H_0. For $z_1 > 3$, $(H_0/c)a_0 r(z_1) \simeq 1.5 + 1.9[1-2/(1+z_1)^{1/2}]$ to better than 2 percent accuracy. The approximation $\dot{n}_h^{\rm com} = (dn_h^{\rm com}/dz)(dz/dt)$ was made, although this could be modified by allowing for merger histories. In the final line, the integral in the line previous was neglected as was the halo density at $z = z_2$. A factor $1/(1+z)$ has been included to account for time-dilation.

We find formation rates for haloes $M > 10^7\, h^{-1}\,{\rm M}_\odot$ and $z > 20$ of $0.0016\,{\rm deg}^{-2}\,{\rm yr}^{-1}$, and $0.20\,{\rm deg}^{-2}\,{\rm yr}^{-1}$ at $z > 10$. These amount to about 70 to 8000 collapsing haloes per year over the sky. The rates are comparable to recent predictions for the total production rate of Pop III pair instability supernovae, with progenitor masses between $140 - 260\,{\rm M}_\odot$, based on cosmological simulations (e.g. Hummel et al. 2012; Johnson et al. 2012), assuming one PI SN per minihalo formed. On the other hand, small scale simulations suggest fragmentation may prevent the formation of Pop III stars sufficiently massive to form a PI SN (e.g. Stacy et al. 2010), although subsequent mergers of the protostars into more massive ones cannot be ruled out. The star formation may also be stochastic given the low number of massive stars formed, with hypernovae forming before a more massive PI SN progenitor is created.

The effect of multiple supernovae on the gas in small haloes is unknown. The heat input of a supernova is sufficient to unbind the IGM of a minihalo with mass below $\sim 10^7\,{\rm M}_\odot$, while, once the gas cools, it will fall back in a more massive system (Whalen et al. 2008; Meiksin 2011). The remaining massive stars will further replenish the IGM through winds, so a gaseous environment may continue to persist on which further supernovae may impact, producing synchrotron emitting remnants. If each halo gives rise to at least one supernova with progenitor mass exceeding $40\,{\rm M}_\odot$, its remnant should then be detectable by eVLA or eMERLIN. If each produces one with a progenitor mass exceeding $15\,{\rm M}_\odot$, SKA should be able to detect the remnant.

An estimate of the expected number counts of radio emitting remnants requires modelling the remnants over a broad redshift range. In the absence of simulations covering a wide range, we use those discussed above, presuming the behaviour of the gas is not very sensitive to redshift. This is a coarse approximation, as the gas content of the haloes is expected to be sensitive to the redshift of their formation. On the other hand, since much of the gas into which the supernova explodes is produced by stellar winds, the environment of the progenitor may not be very redshift dependent. An improved estimate would require a better understanding of star formation within primordial haloes.

The number of sources with observed flux exceeding f_ν is given by modifying equation (5) to account for the duration $\delta t_{f_\nu}^{\rm eff}(z)$ the remnant is visible with a flux exceeding f_ν:

$$N(>f_\nu) = -\int_{z_1}^{z_2} dz\, \frac{dn_h^{\rm com}}{dz} c(a_0 r)^2 \delta t_{f_\nu}^{\rm eff}(z)\delta\Omega. \quad (6)$$

The resulting number counts for haloes collapsing at $z > 20$ are shown in Fig. 6, based on one $40\,{\rm M}_\odot$ hypernova per collapsing halo with a mass exceeding $10^7\, h^{-1}\,{\rm M}_\odot$. The counts are fairly flat up to 5 μJy. A source brighter than 1 μJy should be visible every 50 square degrees, while one source brighter than 1 nJy should be visible per 10 square degrees. At the earliest epochs of star formation, although the remnants would still have observed peak fluxes brighter than 1 μJy, the frequency of their occurrence becomes very small. Only one remnant at $z > 30$ brighter than 1 nJy is expected over the entire sky.

Johnson et al. (2012) suggest Pop III star formation may persist to $z < 10$. This substantially boosts the counts to a few per square degree brighter than 1 μJy, and more than 10 per square degree brighter than 1 nJy. The sources may be identified by their radio colours. Even more definitive, however, would be a survey campaign with repeat multiband observations extended over several years to trace the light curves.

The corresponding number counts based on one $15\,{\rm M}_\odot$ Type II supernova per collapsing halo are shown in Fig. 7. While the fluxes are considerably weaker than for the more energetic hypernovae, the numbers are lower as well as a result of their shorter durations. To detect the remnants at $z > 20$, 200–300 square degree fields would be required to detect remnants as weak as 1 nJy. The counts for $z > 10$ are considerably higher, requiring now 1–2 square degree fields to detect the supernova remnants.

We have also examined the radio absorption signature of the remnants against a bright background radio source. While synchrotron absorption will produce a strong absorption feature at rest frame frequencies below 20 GHz, it lasts less than ~ 100 yr. The number of detectable features along a line of sight will be

$$\frac{dN(>\tau_\nu)}{dz} = n_h^{\rm com}\pi(r_0^{\rm com})^2(1+z)c\delta t_{\tau_\nu}^{\rm eff}(z), \quad (7)$$

where $r_0^{\rm com}$ is the comoving radius of the remnant out to which the line-of-sight absorption optical depth exceeds τ_ν and $\delta t_{\tau_\nu}^{\rm eff}(z)$ is the effective duration of the feature. For a characteristic comoving radius of ~ 1 pc, $dN/dz \sim 3\times 10^{-14}$ at $z = 10$, so that the feature would be undiscoverable. At late times, at $t \sim 0.8$ Myr, the outflowing gas cools sufficiently to produce a 21cm absorption feature that would

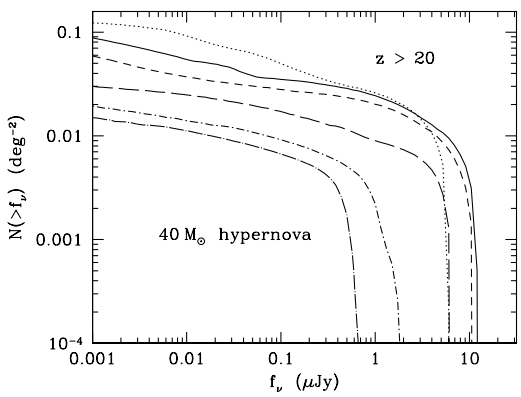

Figure 6. Number counts of radio remnants above a given flux, based on radio light curves for a $40\,M_\odot$ hypernova in $1.2\times10^7\,M_\odot$ minihaloes (for $p_e = 2$, $\gamma_u = 300$ and $f_e = 0.01$) at $z > 20$ (upper panel) and $z > 10$ (lower panel). The observed counts are shown for bands: 0.5 (dotted), 1.4 (solid), 3 (short-dashed), 10 (long-dashed), 25 (dot short-dashed) and 35 (dot long-dashed) GHz. The counts at 25 and 35 GHz would be close to those at 10 GHz for $\gamma_u > 1000$.

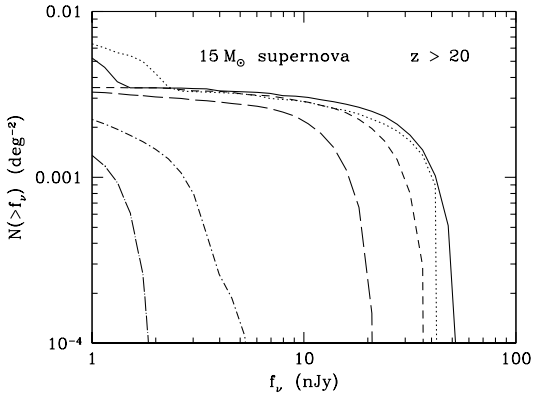

Figure 7. Number counts of radio remnants above a given flux, based on radio light curves for a $15\,M_\odot$ Type II supernova in $1.2\times10^7\,M_\odot$ minihaloes (for $p_e = 2$, $\gamma_u = 300$ and $f_e = 0.01$) at $z > 20$ (upper panel) and $z > 10$ (lower panel). The observed counts are shown for bands: 0.5 (dotted), 1.4 (solid), 3 (short-dashed), 10 (long-dashed), 25 (dot short-dashed) and 35 (dot long-dashed) GHz. The counts at 25 and 35 GHz would be close to those at 10 GHz for $\gamma_u > 1000$.

be measurabe by SKA. We find a characteristic 21cm absorption doublet arising from the cooling shell would form along lines of sight within ~ 5 pc (proper) of the centre of the minihalo. The feature would survive about 1 Myr before transforming into a singlet absorption feature indistinguishable from those expected from minihaloes. This corresponds to $dN/dz \sim 10^{-6}$, again too small to be discovered as there would still not be nearly an adequate number of bright background radio sources to have a fair chance of seeing even one feature.

4 CONCLUSIONS

We estimate the radio signatures of Pop III supernovae in $\sim 10^7\,M_\odot$ minihaloes, sufficiently massive to retain their baryons and form supernova remnants, based on hydrodynamical computations of $15\,M_\odot$ Type II supernovae, $40\,M_\odot$ hypernovae and $260\,M_\odot$ pair instability supernovae at $z = 17.3$ within the haloes. We model the synchrotron emission and absorption assuming a power-law distribution of relativistic electron energies with a total energy density proportional to the thermal energy of the ionized gas, and

equipartition between the relativistic electron and magnetic field energies. Allowing for a relativistic electron component with total energy one percent of the gas thermal energy is sufficient for a hypernova to produce observable fluxes at $0.5 - 35$ GHz exceeding $1\,\mu$Jy, and for the less massive Type II supernova to produce observable fluxes exceeding 10 nJy at $0.5 - 25$ GHz. The PI SN expels much of the halo gas, leaving behind a supernova remnant that produces fluxes of at most 0.1 nJy. A halo mass exceeding $10^8\,h^{-1}\,\mathrm{M}_\odot$ would be sufficient to retain the baryons following a PI SN. Although we do not currently have computations of PI SN in such massive haloes, we may estimate their formation rates: $0.011\,\mathrm{deg}^{-2}\,\mathrm{yr}^{-1}$ if forming at $z > 10$, and $9.1 \times 10^{-6}\,\mathrm{deg}^{-2}\,\mathrm{yr}^{-1}$ for those forming at $z > 20$. These are about a factor 20–200 smaller than the formation rates of minihaloes with masses exceeding $10^7\,h^{-1}\,\mathrm{M}_\odot$, but would still produce a detectable yield of PI SNe remnants over the sky provided their synchrotron fluxes were sufficiently high.

Hypernovae produce observed light curves that rise gradually over a period of 100 yrs, before declining after 200–300 yrs. By contrast, the Type II curves have rise times of 10–20 yrs, and decline abruptly after 30 yrs. The 500 MHz flux lags the higher frequency bands for both supernovae and dominates the emission at its peak as the synchrotron spectrum reddens due to the weakening of the supernova shock. Light curves computed with and without the hypothesized Razin-Tsytovich effect show that the observed 500 MHz flux is substantially diminished by the effect, suggesting it may provide a useful means of testing for its existence.

Estimating the number counts of the supernovae from the minihalo formation rate at $z > 20$, we find a supernova formation rate of about one per 600 square degrees per year. If the supernovae are able to form down to $z = 10$, the rate increases to one per 5 square degrees per year. On average, one $z > 20$ hypernova radio remnant with flux exceeding $1\,\mu$Jy should be detectable at any given time per 50 square degree field, and one with a flux above 1 nJy per 10 square degree field. If Pop III star formation persists to $z < 10$, then a few hypernova remnants brighter than $1\,\mu$Jy would be visible per square degree, and more than ten per square degree brighter than 1 nJy.

Because of their smaller explosion energies, Type II supernovae will produce weaker radio remnants with shorter durations. Fields of 200–300 square degrees would be required to detect remnants forming at $z > 20$ with fluxes above 1 nJy. The numbers are much improved for supernovae forming at $z > 10$, requiring instead 1–2 square degree fields to detect their radio remnants.

Pop III supernova remnants with radio fluxes exceeding $1\,\mu$Jy should be visible in radio surveys using the eVLA or eMERLIN. Weaker few nJy sources would be detectable by the SKA in large numbers. An observing campaign extended over several years would be able to follow the light curves, yielding invaluable data on the formation of the first stars in the Universe and their impact on their local environments.

The readily distinguishable differences between the radio light curves of hypernova and Type II supernova remnants provide the possibility of exploiting the radio emission to infer the initial mass function of the first stars. The frequency with which these explosions are detected over the sky will also constrain Pop III star formation rates through cosmic time along with all-sky NIR surveys by *WFIRST* and *WISH* and deep-field surveys by *JWST*. Their discovery in the radio will permit followup by deep-field observations of the host galaxies by *JWST* and the TMT. Surveys detecting Pop III radio remnants at $10 < z < 15$ may also constrain the multiplicity of their occurrence within individual primeval galaxies, and even the large-scale distribution of the galaxies themselves. The detection of primordial supernova remnants will be one of the most spectacular discoveries in high-redshift radio astronomy in the coming decade.

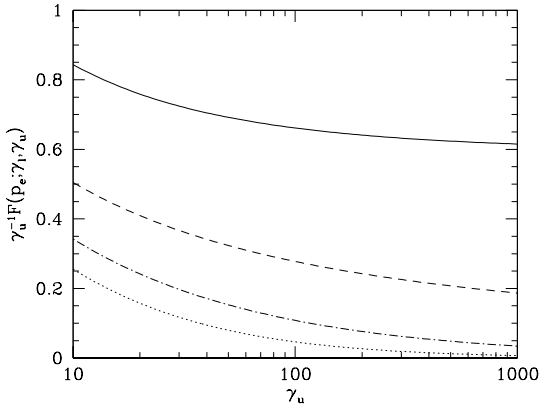

Figure A1. Synchrotron function $F(p_e;\gamma_l,\gamma_u)$ for relativistic electron power-law energy distribution over $\gamma_l < \gamma < \gamma_u$ with index p_e. Shown for $p_e = 1.5$ (solid line), $p_e = 2.0$ (dashed line), $p_e = 2.5$ (dot-dashed line) and $p_e = 3.0$ (dotted line). (A value $\gamma_l = 1$ is adopted.)

APPENDIX A: SYNCHROTRON EMISSION AND ABSORPTION

The synchrotron emissivity for a power-law relativistic electron energy distribution with index p_e extending between the γ factors $\gamma_l < \gamma < \gamma_u$ may be expressed concisely as

$$\epsilon_\nu = \begin{cases} \frac{3-p_e}{2}\frac{\epsilon_{\rm bol}}{\nu_c}\left(\frac{\nu}{\nu_c}\right)^{-\frac{p_e-1}{2}} & ;\frac{1}{3} < p_e < 3 \\ \frac{1}{\log(\nu_c/\nu_{\rm min})}\frac{\epsilon_{\rm bol}}{\nu_c}\left(\frac{\nu}{\nu_c}\right)^{-1} & ;p_e = 3, \end{cases} \tag{A1}$$

where ν_c is the synchrotron upper cutoff frequency

$$\nu_c = \frac{3}{4\pi}\frac{\gamma_u^2 eB\sin\alpha}{m_e c} \tag{A2}$$

for pitch angle α, and $\epsilon_{\rm bol}$ is the bolometric emissivity

$$\epsilon_{\rm bol} = u_B \tau_{\rm se}^{-1} F(p_e;\gamma_l,\gamma_u). \tag{A3}$$

Here, u_B is the energy density of the magnetic field, the characteristic electron scattering time $\tau_{\rm se}$ is given by equation (2) and the function $F(p_e;\gamma_l,\gamma_u)$, shown in Fig. A1,

is

$$F(p_e;\gamma_l,\gamma_u) = 3^{1/2}\frac{9}{4\pi}\frac{2^{(p_e-1)/2}}{p_e+1}\Gamma\left(\frac{p_e}{4}+\frac{19}{12}\right)\Gamma\left(\frac{p_e}{4}-\frac{1}{12}\right) \times \begin{cases} \frac{2-p_e}{3-p_e}\gamma_u\frac{1-(\gamma_l/\gamma_u)^{3-p_e}}{1-(\gamma_l/\gamma_u)^{2-p_e}} & ;p_e\neq 2, p_e\neq 3 \\ \gamma_u\frac{1-\gamma_l/\gamma_u}{\log(\gamma_u/\gamma_l)} & ;p_e=2 \\ \gamma_l\gamma_u\frac{\log(\gamma_u/\gamma_l)}{\gamma_u-\gamma_l} & ;p_e=3. \end{cases} \quad \text{(A4)}$$

The inverse attenuation length due to synchrotron self-absorption may be expressed as

$$\alpha_\nu = r_0^{-1}\left(\frac{1}{\nu_c\tau_{\rm se}}\right)\left(\frac{\nu_c}{\nu}\right)^{(p_e+4)/2}G(p_e;\gamma_l,\gamma_u), \quad \text{(A5)}$$

where r_0 is the classical electron radius and

$$G(p_e;\gamma_l,\gamma_u) = \frac{3^{1/2}}{16\pi}\frac{2^{p_e/2}}{\gamma_u^4}\Gamma\left(\frac{p_e}{4}+\frac{1}{6}\right)\Gamma\left(\frac{p_e}{4}+\frac{11}{6}\right) \times \begin{cases} \frac{2-p_e}{1-(\gamma_l/\gamma_u)^{2-p_e}} & ;p_e\neq 2 \\ \frac{1}{\log(\gamma_u/\gamma_l)} & ;p_e=2. \end{cases} \quad \text{(A6)}$$

ACKNOWLEDGMENTS

We thank Jim Dunlop and Jeff Peterson for valuable discussions. DJW was supported by the Bruce and Astrid McWilliams Center for Cosmology at Carnegie Mellon University. All ZEUS-MP simulations were performed on Institutional Computing (IC) platforms at LANL (Coyote).

REFERENCES

Abel T., Bryan G. L., Norman M. L., 2002, Science, 295, 93
Abel T., Wise J. H., Bryan G. L., 2007, ApJ, 659, L87
Alvarez M. A., Bromm V., Shapiro P. R., 2006, ApJ, 639, 621
Beers T. C., Christlieb N., 2005, ARA&A, 43, 531
Bromm V., Coppi P. S., Larson R. B., 2002, ApJ, 564, 23
Bromm V., Yoshida N., Hernquist L., 2003, ApJ, 596, L135
Cayrel R., Depagne E., Spite M., Hill V., Spite F., François P., Plez B., Beers T., Primas F., Andersen J., Barbuy B., Bonifacio P., Molaro P., Nordström B., 2004, A&Ap, 416, 1117
Chevalier R. A., 1982, ApJ, 259, 302
Chevalier R. A., 1998, ApJ, 499, 810
Chiaki G., Yoshida N., Kitayama T., 2012, ArXiv e-prints, 1203.0820
Clark P. C., Glover S. C. O., Smith R. J., Greif T. H., Klessen R. S., Bromm V., 2011, Science, 331, 1040
Fomalont E. B., Kellermann K. I., Partridge R. B., Windhorst R. A., Richards E. A., 2002, AJ, 123, 2402
Frebel A., Aoki W., Christlieb N., et al. 2005, Nature, 434, 871
Furlanetto S. R., Loeb A., 2002, ApJ, 579, 1
Greif T. H., Bromm V., Clark P. C., Glover S. C. O., Smith R. J., Klessen R. S., Yoshida N., Springel V., 2012, MNRAS, 424, 399
Greif T. H., Glover S. C. O., Bromm V., Klessen R. S., 2010, ApJ, 716, 510
Greif T. H., Johnson J. L., Bromm V., Klessen R. S., 2007, ApJ, 670, 1
Greif T. H., Johnson J. L., Klessen R. S., Bromm V., 2008, MNRAS, 387, 1021
Greif T. H., Springel V., White S. D. M., Glover S. C. O., Clark P. C., Smith R. J., Klessen R. S., Bromm V., 2011, ApJ, 737, 75
Hasegawa K., Umemura M., Susa H., 2009, MNRAS, 395, 1280
Heger A., Woosley S. E., 2002, ApJ, 567, 532
Hosokawa T., Omukai K., Yoshida N., Yorke H. W., 2011, Science, 334, 1250
Hummel J. A., Pawlik A. H., Milosavljević M., Bromm V., 2012, ApJ, 755, 72
Iliev I. T., Shapiro P. R., Ferrara A., Martel H., 2002, ApJ, 572, L123
Iliev I. T., Shapiro P. R., Raga A. C., 2005, MNRAS, 361, 405
Iwamoto N., Umeda H., Tominaga N., Nomoto K., Maeda K., 2005, Science, 309, 451
Joggerst C. C., Almgren A., Bell J., Heger A., Whalen D., Woosley S. E., 2010, ApJ, 709, 11
Johnson J. L., Dalla Vecchia C., Khochfar S., 2012, ArXiv e-prints, 1206.5824
Johnson J. L., Greif T. H., Bromm V., 2008, MNRAS, 388, 26
Kitayama T., Yoshida N., 2005, ApJ, 630, 675
Kitayama T., Yoshida N., Susa H., Umemura M., 2004, ApJ, 613, 631
Komatsu E., Dunkley J., Nolta M. R., Bennett C. L., Gold B., Hinshaw G., Jarosik N., Larson D., Limon M., Page L., Spergel D. N., Halpern M., Hill R. S., Kogut A., Meyer S. S., Tucker G. S., Weiland J. L., Wollack E., Wright E. L., 2009, ApJS, 180, 330
Lai D. K., Bolte M., Johnson J. A., Lucatello S., Heger A., Woosley S. E., 2008, ApJ, 681, 1524
Mackey J., Bromm V., Hernquist L., 2003, ApJ, 586, 1
Meiksin A., 2011, MNRAS, 417, 1480
Moriya T. J., Blinnikov S. I., Tominaga N., Yoshida N., Tanaka M., Maeda K., Nomoto K., 2012, ArXiv e-prints, 1204.6109
Muxlow T. W. B., Richards A. M. S., Garrington S. T., Wilkinson P. N., Anderson B., Richards E. A., Axon D. J., Fomalont E. B., Kellermann K. I., Partridge R. B., Windhorst R. A., 2005, MNRAS, 358, 1159
Nagakura T., Hosokawa T., Omukai K., 2009, MNRAS, 399, 2183
Nakamura F., Umemura M., 2001, ApJ, 548, 19
Oh S. P., Cooray A., Kamionkowski M., 2003, MNRAS, 342, L20
O'Shea B. W., Norman M. L., 2007, ApJ, 654, 66
O'Shea B. W., Norman M. L., 2008, ApJ, 673, 14
Owen F. N., Morrison G. E., 2008, AJ, 136, 1889
Pan T., Kasen D., Loeb A., 2011, ArXiv e-prints, 1112.2710
Reed D. S., Bower R., Frenk C. S., Jenkins A., Theuns T., 2007, MNRAS, 374, 2
Rybicki G. B., Lightman A. P., 1986, Radiative Processes in Astrophysics. Wiley, 1986
Scannapieco E., Madau P., Woosley S., Heger A., Ferrara A., 2005, ApJ, 633, 1031
Schaerer D., 2002, A&Ap, 382, 28
Scheuer P. A. G., Williams P. J. S., 1968, ARA&A, 6, 321

Shapiro P. R., Ahn K., Alvarez M. A., Iliev I. T., Martel H., Ryu D., 2006, ApJ, 646, 681
Shapiro P. R., Iliev I. T., Raga A. C., 2004, MNRAS, 348, 753
Smith B. D., Sigurdsson S., 2007, ApJ, 661, L5
Smith B. D., Turk M. J., Sigurdsson S., O'Shea B. W., Norman M. L., 2009, ApJ, 691, 441
Soderberg A. M., Chevalier R. A., Kulkarni S. R., Frail D. A., 2006, ApJ, 651, 1005
Stacy A., Greif T. H., Bromm V., 2010, MNRAS, 403, 45
Stacy A., Greif T. H., Bromm V., 2011, ArXiv e-prints, 1109.3147
Susa H., Umemura M., 2006, ApJ, 645, L93
Susa H., Umemura M., Hasegawa K., 2009, ApJ, 702, 480
Tanaka M., Moriya T. J., Yoshida N., Nomoto K., 2012, MNRAS, 422, 2675
Turk M. J., Abel T., O'Shea B., 2009, Science, 325, 601
Weiler K. W., Sramek R. A., Panagia N., van der Hulst J. M., Salvati M., 1986, ApJ, 301, 790
Whalen D., Abel T., Norman M. L., 2004, ApJ, 610, 14
Whalen D., Hueckstaedt R. M., McConkie T. O., 2010, ApJ, 712, 101
Whalen D., O'Shea B. W., Smidt J., Norman M. L., 2008, ApJ, 679, 925
Whalen D., van Veelen B., O'Shea B. W., Norman M. L., 2008, ApJ, 682, 49
Whalen D. J., 2012, The First Stars, Proceedings of Vulcano 2012: Frontiers in Astrophysics and Particle Physics
Wise J. H., Abel T., 2007, ApJ, 671, 1559
Wise J. H., Turk M. J., Norman M. L., Abel T., 2012, ApJ, 745, 50
Woosley S. E., Blinnikov S., Heger A., 2007, Nature, 450, 390
Yoshida N., Oh S. P., Kitayama T., Hernquist L., 2007, ApJ, 663, 687